*nanomaterials*

MDPI

*Article*

# Precise Control of Green to Blue Emission of Halide Perovskite Nanocrystals Using Terbium Chloride as Chlorine Source

**Wenqiang Deng [1], Ting Fan [1,*], Jiantao Lü [2,*], Jingling Li [1], Tingting Deng [2] and Mingqi Liu [1]**

[1] School of Materials Science and Hydrogen Energy, Foshan University, Foshan 528000, China; wenqiangdeng000@163.com (W.D.); lijl@fosu.edu.cn (J.L.); polop000@163.com (M.L.)
[2] School of Physics and Optoelectronic Engineering, Foshan University, Foshan 528000, China; tingtingdeng0803@163.com
* Correspondence: fanting@fosu.edu.cn (T.F.); keentle@gmail.com (J.L.)

**Abstract:** $CsPbCl_xBr_{3-x}$ nanocrystals were prepared by ligand-assisted deposition at room temperature, and their wavelength was accurately adjusted by doping $TbCl_3$. The synthesized nanocrystals were monoclinic and the morphology was almost unchanged after doping. The fluorescence emission of $CsPbCl_xBr_{3-x}$ nanocrystals was easily controlled from green to blue by adjusting the amount of $TbCl_3$, which realizes the continuous and accurate spectral regulation in the range of green to blue. This method provides a new scheme for fast anion exchange of all-inorganic perovskite nanocrystals in an open environment at room temperature.

**Keywords:** room temperature assisted recrystallization; nanocrystalline; spectrum control

check for updates

**Citation:** Deng, W.; Fan, T.; Lü, J.; Li, J.; Deng, T.; Liu, M. Precise Control of Green to Blue Emission of Halide Perovskite Nanocrystals Using Terbium Chloride as Chlorine Source. *Nanomaterials* **2021**, *11*, 2390. https://doi.org/10.3390/nano11092390

Academic Editor: Ashish Arora

Received: 22 July 2021
Accepted: 1 September 2021
Published: 14 September 2021

**Publisher's Note:** MDPI stays neutral with regard to jurisdictional claims in published maps and institutional affiliations.

**Copyright:** © 2021 by the authors. Licensee MDPI, Basel, Switzerland. This article is an open access article distributed under the terms and conditions of the Creative Commons Attribution (CC BY) license (https://creativecommons.org/licenses/by/4.0/).

## 1. Introduction

All inorganic cesium lead halide perovskite $CsPbX_3$ (X = Cl, Br and I) quantum dots have excellent optoelectronic properties, such as excellent defect tolerance, long carrier life, a large absorption cross-section, high photoluminescence quantum yield, narrow emission peak, and adjustable emission in the visible spectrum range. It has a good application prospect in optoelectronic devices [1–3]. In 2015, Protesescu et al. first proposed the thermal injection method for the preparation of inorganic perovskite quantum dots [4]. By discarding the supernatant and re-dispersing in toluene or n-hexane to form a stable $CsPbX_3$ nanocrystalline colloidal solution, perovskite nanocrystals with controllable morphologies, including quantum dots, nanowires, nanosheets, and nanorods, can be prepared [5–9]. However, this method requires the preparation of cesium oleate precursors, followed by rapid injection of lead halide precursors at high temperatures. The synthesis method requires high-temperature heating and inert gas protection, which greatly limits the application of perovskite quantum dots in practical applications.

In 2016, Li et al. prepared $CsPbX_3$ nanocrystals by room-temperature ligand-assisted deposition (LARP), which is different from thermal-injection synthesis [10]. The process involves dissolving perovskite precursors, oleic acid, oleamine, etc., in a polar N, N-dimethylformamide (DMF) solvent, rather than the ODE used in the thermal injection method, and gradually adding a certain amount of the precursor solution to toluene or n-hexane under intense agitation. The salts commonly used in LARP methods are $PbX_2$ and CsX. The mixing of the two solvents causes instantaneous monomer supersaturation, which triggers nucleation and growth of perovskite nanocrystals. Because the LARP process is performed in the air with a simple agitator opening, it can be scaled up to produce perovskite nanocrystals on a large scale, even up to the grade of gram [11,12]. In addition, the optical properties of $CsPbX_3$ nanocrystals prepared by the room-temperature precipitation method are close to those prepared by the thermal injection method, although the reaction temperature is low and there is no inert atmosphere to protect the nanocrystals [13–16].

Different from traditional semiconductor quantum dots, the average size of $CsPbX_3$ nanocrystals (NCs) is usually larger than 10 nm, larger than its exciton Bohr radius, so it is difficult to achieve continuous fluorescence emission only through size adjustment [17–19]. Thanks to the unique anion exchange characteristics and high ion mobility of $CsPbX_3$ nanocrystals, fluorescence emission wavelength tuning of full visible-spectrum emission can be achieved by exchanging nanocrystalline halogen ions (Cl, Br or I) [20–23]. However, the traditional anion exchange reaction using $PbCl_2$ needs to undergo complex pretreatment, excessive ligand-induced degradation of nanocrystals, and incomplete ionization of $PbCl_2$ salts. These will result in unpredictable fluorescence shifts and cannot be tuned quantitatively and accurately [24]. For example, if excessive oleamine (OLA) is used, $CsPbBr_3$ NCs will be partially or completely converted to $Cs_4PbBr_6$ NCs [25]. The addition of alkyl ammonium bromide in the anion exchange process will also lead to the unexpected evolution of the $CsPb_2Br_5$ perovskite phase. In this regard, the key to accurate emission control of $CsPbX_3$ NCS is to establish a programmed and accurate anion exchange route with high halide ion reactivity to prepare pure phase $CsPbX_3$ NCs [26]. In the anion exchange process, some efforts have been made to improve the reactivity of halides. Benzoyl halides and trimethylsilyl halides are electrophilic reagents. They show high reactivity in the anion exchange reaction by destroying halogen bonds, releasing halide ions, and promoting the substitution of halide components in $CsPbX_3$ NCS, although these reagents are toxic [27,28]. The environmentally friendly metal halide solid $MX_2$ (M = Zn, Ni and Mg) is also used as a halide source to achieve rapid anion exchange at room temperature [29,30]. The inorganic halide salt greatly simplifies the reaction process and speeds up the reaction rate. However, in the process of inorganic halide exchange, with the opening of rigid halide octahedron structure around lead, partial cation exchange of metal cations to lead is likely to occur. Different from the traditional anion exchange method, in 2019, Liu et al. dissolved $ZnX_2$ in water, and the prepared $ZnX_2$ aqueous solution was used as the halide source in anion exchange. The fluorescence emission peak position of $CsPbX_3$ nanocrystals can be adjusted continuously and accurately in the whole visible spectrum [25]. However, due to the introduction of water, the nanocrystals will inevitably dissociate. In 2020, Pan et al. introduced a $NiCl_2$ solution into the $CsPbBr_3$ reaction medium, where the emission wavelength was in the range of 508–432 nm and its PLQY reached 89%. However, $Ni^{2+}$ inevitably entered the Pb lattice, resulting in changes in the structure, thus affecting its optical properties and uncontrollable factors for accurately regulating the fluorescence spectrum band [30].

All-inorganic mixed halide perovskite is often used to obtain blue LEDs with shorter emission wavelengths. For example, Zheng and his collaborators recently reported the preparation of all-inorganic $CsPb(Cl/Br)_3$ Perovskite blue led by the thermal injection method, and obtained perovskite lead with a luminous wavelength of 470 nm and efficiency of 6.3% [31]. In this study, we reported the successful synthesis of $CsPbCl_xBr_{3-x}$ nanocrystals at room temperature by an improved supersaturated reprecipitation method by introducing different amounts of $TbCl_3$ solution into the reaction medium. The fluorescence emission peak position of the synthesized $CsPbCl_xBr_{3-x}$ nanocrystals is adjustable in the range of 431 nm to 512 nm and has good phase/chemical stability. Experiments show that the fluorescence emission of $CsPbX_3$ nanocrystals can be accurately and continuously regulated like traditional semiconductor nanocrystals, making perovskite nanocrystals more competitive in lighting and display applications.

## 2. Experiments

### *2.1. Experimental Materials*

The experimental materials include cesium bromide (CsBr, analytically pure, purity 99.5%); $PbBr_2$ (analytically pure, purity 99.0%), terbium trichloride, hexahydrate ($TbCl_3.6H_2O$, analytically pure, purity 99.9%); Oleic acid (purity 85%); Oleylamine (80~90% purity); N,N-dimethylformamide (DMF, analytically pure, 99.5%); and toluene, all of which were not further purified.

### 2.2. Synthesis of $CsPbCl_xBr_{3-x}$ Nanocrystalline

The all-inorganic perovskite $CsPbBr_3$ was synthesized by room-temperature supersaturation recrystallization. Under the condition of magnetic stirring and heating, 0.4 mmol CsBr, 0.4 mmol $PbBr_2$, 1 mL oleic acid, and 0.5 mL oleylamine were dissolved in 10 mL DMF as the sources of Cs, Pb, and Br. Only 1 mL of the $PbBr_2$/CsBr solution was slowly injected into 10 mL of toluene under ultrasonic conditions. After a few seconds, bright green light emission was observed under UV irradiation of 365 nm.

Synthesis of $CsPbCl_xBr_{3-x}$ nanocrystals: Firstly, 1 mmol $TbCl_3.6H_2O$ was dissolved in 1 mL DMF as a Cl source under magnetic stirring. Then 5, 10, 20, 40, and 80 µL $TbCl_3$ solutions were added dropwise, followed by 1 mL of the above-mentioned $PbBr_2$/CsBr mixture solution and 10 mL of toluene. The process was carried out under ultrasound. After a few seconds, green and blue light emission was observed under the irradiation of an ultraviolet ray at 365 nm. The nanocrystals with the addition of 5, 10, 20, 40, and 80 µL $TbCl_3$ solutions represent $CsPbCl_{0.33}Br_{2.67}$, $CsPbCl_{0.6}Br_{2.4}$, $CsPbCl_1Br_2$, $CsPbCl_{1.5}Br_{1.5}$, and $CsPbCl_2Br_1$, respectively.

### 2.3. Purifications

The nanocrystals synthesized at room temperature were centrifuged at 3000 r/min for 5 min, and the supernatant was retained. Then, the supernatant was centrifuged at 11,000 r/min for 15 min, and 3 mL toluene was added to the resulting precipitate, which was further centrifuged at 11,000 r/min for 15 min. The precipitate was retained, and finally it was dispersed into 3 mL toluene for optical performance testing and morphology characterization.

### 2.4. Characterizations

X-ray powder diffraction image (XRD) shows CuKα emission (λ = 1.5418 A) assisted by the Bruker Smart-Apex-II X-Ray Single-Crystal Diffractometer. Transmission Electron Microscope Hitachi H-800 (acceleration voltage of 200 kV) is used for transmission electron microscope image photography. UV-Vis absorption spectra were characterized by the Shimazu -3600 UV-NIR spectrophotometer. The Horiba Fluoromax-4 steady-state and transient fluorescence spectrometer measured the emission spectrum and fluorescence lifetime. X-ray photoelectron spectroscopy (XPS) was measured by the Thermo ESCALAB 250XI spectrometer with Al Ka excitation (1486.6 eV).

## 3. Results and Discussions

As can be seen from Figure 1, the diffraction peaks 15.081, 21.498, 30.698, 37.603, and 43.692 of $CsPbCl_xBr_{3-x}$ nanocrystals with different halogen components correspond to (001), (110), (−200), (121), and (−202) crystal planes of $CsPbBr_3$ (PDF#18-0364) standard card, respectively. Therefore, the nanocrystals possess the crystalline structure of monoclinic bulk $CsPbBr_3$ (PDF#18-0364) [30]. With the increase of $Cl^-$ ion content, the above diffraction peaks gradually move to a large angle, which is caused by the lattice shrinkage caused by the replacement of $Br^-$ (1.96 Å) ions with a larger radius to smaller $Cl^-$ (1.81 Å) ions [32,33]. For the $CsPbX_3$ NCs, monoclinic is a metastable structure, the formation of which is thermodynamically controlled. In the room-temperature ligand-assisted deposition, the reaction temperature is rather low that the total energy is insufficient to overcome the barrier to crystallizing into the tetragonal phase as can be obtained in the hot-injection approach. The existence of the stable metastable phase at low temperature is attributed to the capping ligands (OLA) on the surface of the as- prepared NCs, which lower the surface energy [34].

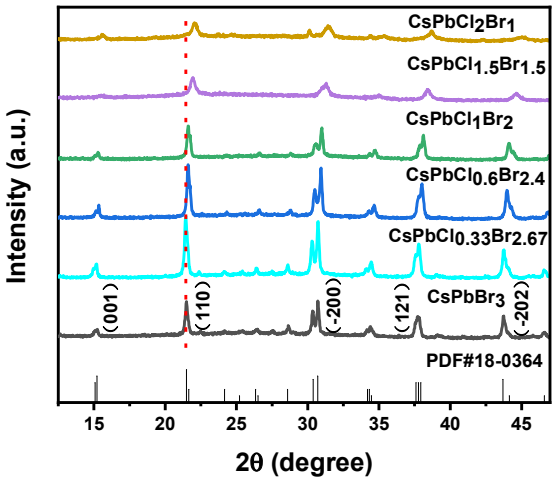


**Figure 1.** XRD patterns of CsPbClxBr3-x nanocrystals with different halogen components.

Figure 2a,b shows TEM images of $CsPbBr_3$ and $CsPbCl_1Br_2$ nanocrystals prepared by supersaturated recrystallization at room temperature. It can be seen from the figures that $CsPbBr_3$ and $CsPbCl_1Br_2$ nanocrystals maintain uniform distribution and exhibit good monodispersion properties. The size of most of them is about 20 nm, showing high dimensional uniformity, and their morphology almost does not change before and after doping.

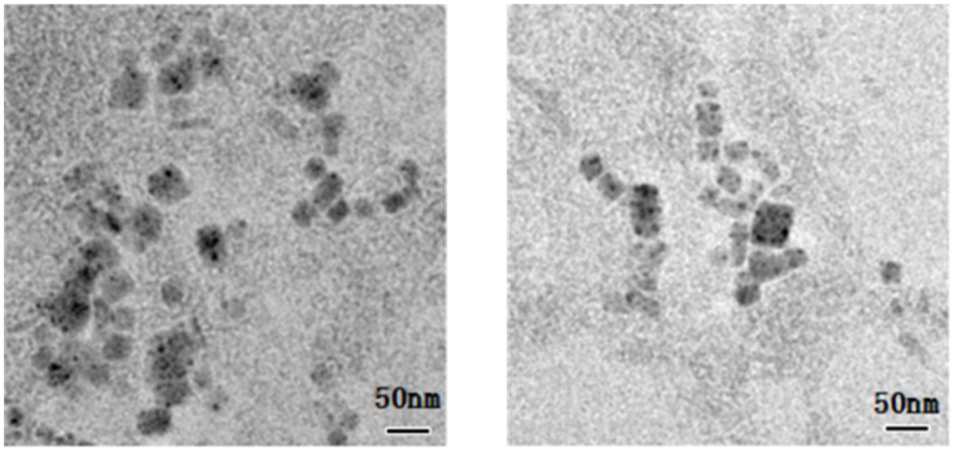


**Figure 2.** (**a**) TEM images of $CsPbBr_3$ nanocrystals and (**b**) $CsPbCl_1Br_2$ nanocrystals.

From the XPS spectrum of Figure 3a–e, the characteristic peaks of Cs 3d, Pb 4d, Pb 4f, Br 3d, and Cl 2p can be clearly observed, among which the characteristic peak of Cl 2p appears, further indicating that the characteristic peak of $Tb^{3+}$ still does not appear in the crystal lattice position of bromine successfully incorporated by the chloride ion under the detection limit of XPS measurement. This means that $Tb^{3+}$ will not be mixed into the lattice position of $CsPbCl_xBr_{3-x}$. This not only avoids the pollution of metal ions when metal halides are used as the halogen source, but also solves the problems of incomplete ionization and toxicity of Pb ions when $PbCl_2$ is traditionally used as the halogen source [35].

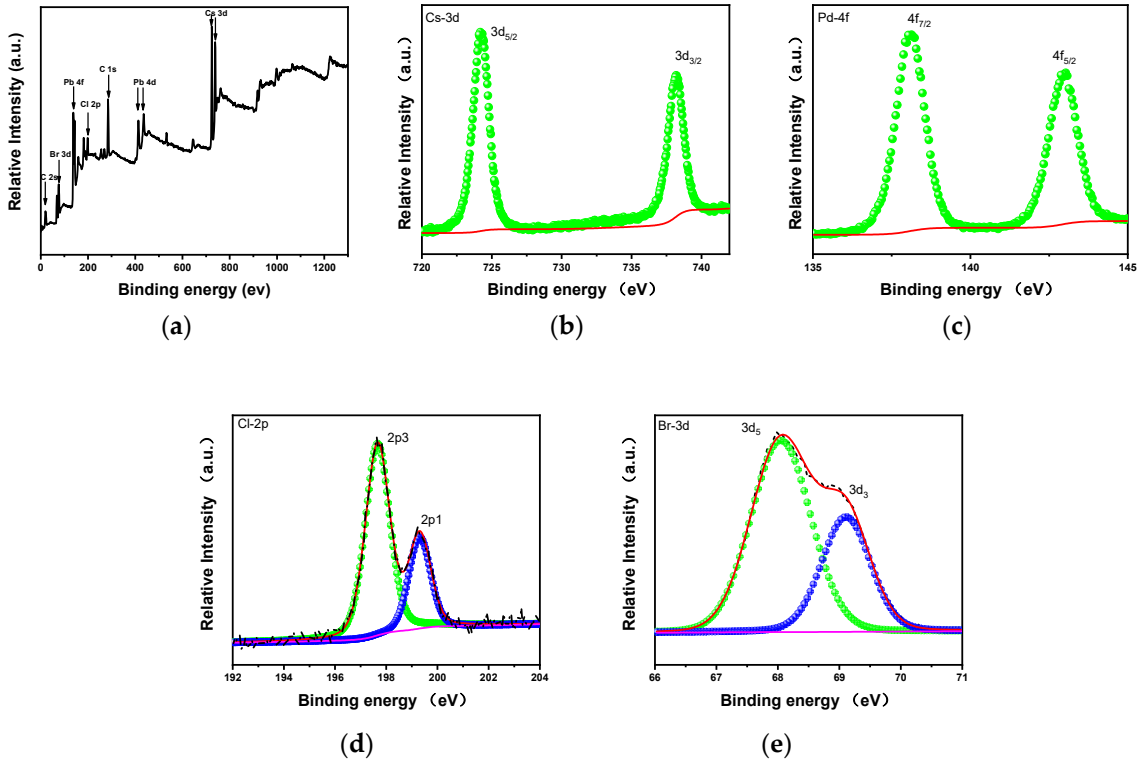


**Figure 3.** (**a**) The XPS spectrum of $CsPbCl_1Br_2$ nanocrystals; (**b**) XPS spectra of Cs 3d in $CsPbCl_1Br_2$ nanocrystals; (**c**) XPS spectra of Pb 4f in $CsPbCl_1Br_2$ nanocrystals; (**d**) XPS spectra of Cl 2p in $CsPbCl_1Br_2$ nanocrystals; (**e**) XPS spectra of Br 3d in $CsPbCl_1Br_2$ nanocrystals.

In order to observe the influence of chloride ion doping on the band gap of $CsPbCl_xBr_{3-x}$ nanocrystals, we measured the absorption spectra of $CsPbCl_xBr_{3-x}$ nanocrystals after adding different amounts of $TbCl_3$, as shown in Figure 4a. It can be seen from the figure that, with the increase of $TbCl_3$ addition, the absorption edge of $CsPbCl_xBr_{3-x}$ moves towards the short-wavelength direction, which is mainly caused by the increase of the band gap of $CsPbCl_xBr_{3-x}$ nanocrystals as $Cl^-$ replaces $Br^-$, corresponding to the blue shift of the fluorescence emission peak position [36]. As shown in Figure 4b, fluorescence emission can be adjusted from 512 nm to 431 nm only by changing the content of doped $TbCl_3$.The nanocrystals can be controlled continuously and accurately from green light to blue light, and the half-peak width of the emission spectrum is very narrow, ranging from 18.1 nm to 34.1 nm. As shown in the inset of Figure 4c, with the increase of $TbCl_3$ addition, the luminescence of the corresponding $CsPbCl_xBr_{3-x}$ nanocrystals under ultraviolet light gradually changes from green to blue. After two weeks, the luminescence brightness of the colloidal dispersion of $CsPbX_3$ nanocrystals remained basically unchanged. The corresponding CIE color coordinates are (0.066, 0.732), (0.066, 0.732), (0.094, 0.166), (0.142, 0.076), (0.154, 0.057), and (0.169, 0.061), respectively. Interestingly, we found similar results when using $EuCl_3$ as the chlorine source, which could be seen in Figures S1 and S2.

As can be seen in Figure 4d, the change of halogen components will lead to the change of average fluorescence lifetime. The overall performance is as follows: With the increase of $Cl^-$ ion content, the fluorescence lifetime will be shortened, and the band gap corresponding to halogen ions is negatively correlated with the attenuation lifetime [37]. When fitting the fluorescence decay lifetime spectrum of $CsPbCl_xBr_{3-x}$, it is found that the fluorescence decay process of the sample conforms to the double exponential decay, and its average fluorescence lifetime is calculated by the following formula:

$$\tau_{av} = \frac{(\alpha_1\tau_1^2 + \alpha_2\tau_2^2)}{(\alpha_1\tau_1 + \alpha_2\tau_2)}$$

Among them, $\tau_i$ and $\alpha_i$ are the weight coefficient and fluorescence lifetime coefficient of PL curve life, respectively. The fluorescence lifetime of $CsPbBr_3$ nanocrystals is up to 65.5 ns. By fitting the fluorescence attenuation lifetime spectrum of $CsPbCl_xBr_{3-x}$, it is found that its fluorescence attenuation process conforms to the three-exponential decay, and its average fluorescence lifetime is calculated by the following formula:

$$\tau_{av} = \frac{\alpha_1\tau_1^2 + \alpha_2\tau_2^2 + \alpha_3\tau_3^2}{\alpha_1\tau_1 + \alpha_2\tau_2 + \alpha_3\tau_3}$$

The fluorescence lifetime of $CsPbCl_{0.33}Br_{2.67}$, $CPbCl_{0.6}Br_{2.4}$, $CsPbCl_1Br_2$, $CsPbCl_{1.5}Br_{1.5}$, and $CsPbCl_2Br_1$ were 56.9 ns, 38.7 ns, 17.9 ns, 8.7 ns, and 4.3 ns, respectively. The luminescence data of $CsPbCl_xBr_{3-x}$ nanocrystals can be seen in Table 1.

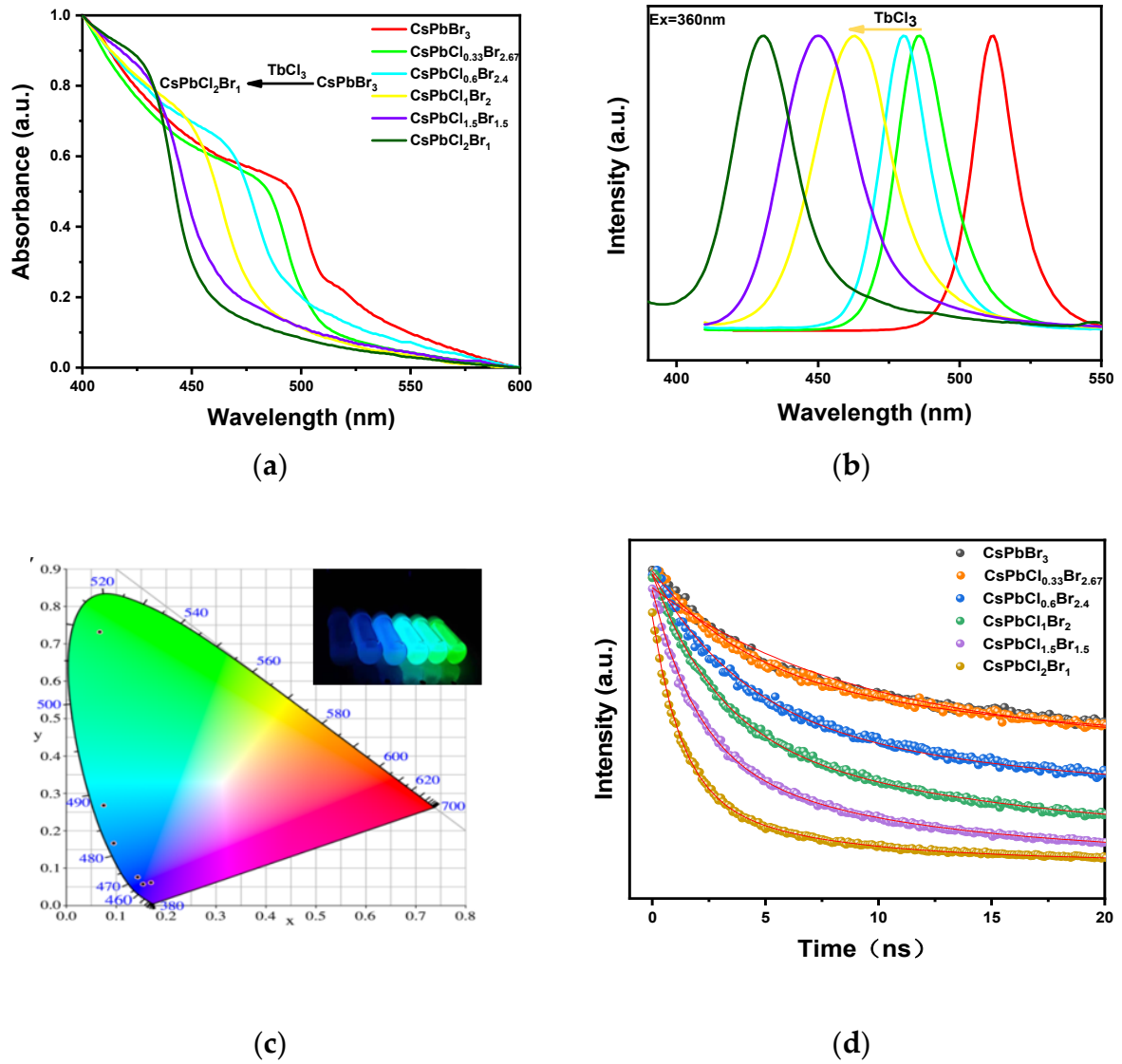


**Figure 4.** (**a**) Ultraviolet absorption spectra of $CsPbCl_xBr_{3-x}$ nanocrystals with different halogen components; (**b**) the fluorescence emission spectra of $CsPbCl_xBr_{3-x}$ nanocrystals with different halogen components (from left to right are $CsPbCl_2Br_1$, $CsPbCl_{1.5}Br_{1.5}$, $CsPbCl_1Br_2$, $CsPbCl_{0.6}Br_{2.4}$, $CsPbCl_{0.33}Br_{2.67}$, and $CsPbBr_3$). (**c**) The CIE diagram of different halogen components of $CsPbCl_xBr_{3-x}$ nanocrystals. The illustration shows the photos of the synthesized $CsPbCl_xBr_{3-x}$ nanocrystals under the ultraviolet lamp; (**d**) fluorescence lifetime diagrams of $CsPbCl_xBr_{3-x}$ nanocrystals with different halogen components.

**Table 1.** Luminescence data of $CsPbCl_xBr_{3-x}$ nanocrystals based on different halogen components.

| The Sample | The Emission Peak | Full Width at Half Height | Mean Fluorescence Lifetime | CIE Coordinates |
|---|---|---|---|---|
| $CsPbBr_3$ | 512 nm | 18.1 nm | 65.5 ns | (0.066, 0.732) |
| $CsPbCl_{0.33}Br_{2.67}$ | 486 nm | 23.1 nm | 56.9 ns | (0.075, 0.269) |
| $CsPbCl_{0.6}Br_{2.4}$ | 480 nm | 20.7 nm | 38.7 ns | (0.094, 0.166) |
| $CsPbCl_1Br_2$ | 463 nm | 34.1 nm | 17.9 ns | (0.142, 0.076) |
| $CsPbCl_{1.5}Br_{1.5}$ | 450 nm | 32.3 nm | 8.7 ns | (0.154, 0.057) |
| $CsPbCl_2Br_1$ | 431 nm | 27.3 nm | 4.3 ns | (0.169, 0.061) |

## 4. Conclusions

In this paper, $CsPbCl_xBr_{3-x}$ nanocrystals were directly synthesized by doping with $TbCl_3$ at room temperature in an open environment. The synthesized $CsPbCl_xBr_{3-x}$ nanocrystals belong to the monoclinic phase and maintain uniform distribution, showing good monodispersion properties. The size of most of them is about 20 nm and their morphology almost does not change before and after doping. By adjusting the amount of $TbCl_3$, the fluorescence emission was accurately adjusted from green to blue. This provides a new scheme for fast anion exchange of perovskite nanocrystals with all-inorganic cesium-lead halide in an open environment at room temperature and has practical application value in the fields of light-emitting diodes, solar cells, and photodetectors.

**Supplementary Materials:** The following are available online at https://www.mdpi.com/article/10.3390/nano11092390/s1, Figure S1: Photo of $CsPbCl_xBr_{3-x}$ nanocrystals under ultraviolet light (from left to right, $CsPbBr_3$, $CsPbCl_{0.15}Br_{2.85}$, $CsPbCl_{0.27}Br_{2.73}$, $CsPbCl_{0.4}Br_{2.6}$, $CsPbCl_{0.82}Br_{2.18}$, $CsPbCl_{1.16}Br_{1.84}$ and $CsPbCl_{1.5}Br_{1.5}$, respectively). Figure S2: Fluorescence emission spectra of $CsPbCl_xBr_{3-x}$ nanocrystals with different halogen components (from left to right, $CsPbCl_{1.5}Br_{1.5}$, $CsPbCl_{1.16}Br_{1.84}$, $CsPbCl_{0.82}Br_{2.18}$, $CsPbCl_{0.4}Br_{2.6}$, $CsPbCl_{0.27}Br_{2.73}$, $CsPbCl_{0.15}Br_{2.85}$ and $CsPbBr_3$, respectively).

**Author Contributions:** T.F. and J.L. (Jiantao Lü) conceived the idea for the research; W.D. and J.L. (Jiantao Lü) performed the simulation; T.F. and W.D. wrote the paper; W.D. performed the experiments; T.F. and J.L. (Jingling Li) analyzed the simulation and proofread the manuscript; All authors contributed in writing the final manuscript. All authors have read and agreed to the published version of the manuscript.

**Funding:** This work is supported by the National Natural Science Foundation of China (No. 51702051 and 51902054), Natural Science Foundation of Guangdong province (Grant No. 2017A030313307), and Foshan inorganic micro-nano luminescent materials engineering technology research center.

**Data Availability Statement:** The data presented in this study are available in this paper.

**Acknowledgments:** This work is supported by the National Natural Science Foundation of China (No. 51702051 and 51902054), Natural Science Foundation of Guangdong province (Grant No. 2017A030313307), and Foshan inorganic micro-nano luminescent materials engineering technology research center. All authors agree to this acknowledgment.

**Conflicts of Interest:** The authors declare no conflict of interest.

## References

1. Huang, H.; Susha, A.S.; Kershaw, S.V.; Hung, T.F.; Rogach, A.L. Control of emission color of high quantum yield $CH_3NH_3PbBr_3$ perovskite quantum dots by precipitation temperature. *Adv. Sci.* **2015**, *2*, 1500194. [CrossRef]
2. Kumawat, N.K.; Dey, A.; Kumar, A.; Gopinathan, S.P.; Narasimhan, K.L.; Kabra, D. Band gap tuning of $CH_3NH_3Pb(Br_{1-x}Cl_x)_3$ hybrid perovskite for blue electroluminescence. *ACS Appl. Mater. Interfaces* **2015**, *7*, 13110–13124. [CrossRef] [PubMed]
3. Righetto, M.; Meggiolaro, D.; Rizzo, A.; Sorrentino, R.; He, Z.; Meneghesso, G.; Sum, T.C.; Gatti, T.; Lamberti, F. Coupling halide perovskites with different materials: From doping to nanocomposites, beyond photovoltaics. *Prog. Mater. Sci.* **2020**, *110*, 100639. [CrossRef]
4. Protesescu, L.; Yakunin, S.; Bodnarchuk, M.I.; Krieg, F.; Caputo, R.; Hendon, C.H.; Yang, R.X.; Walsh, A.; Kovalenko, M.V. Nanocrystals of cesium lead halide perovskites ($CsPbX_3$, X= Cl, Br, and I): Novel optoelectronic materials showing bright emission with wide color gamut. *Nano Lett.* **2015**, *15*, 3692–3696. [CrossRef]

5. Lignos, I.; Stavrakis, S.; Nedelcu, G.; Protesescu, L.; deMello, A.J.; Kovalenko, M.V. Synthesis of cesium lead halide perovskite nanocrystals in a droplet-based microfluidic platform: Fast parametric space mapping. *Nano Lett.* **2016**, *16*, 1869–1877. [CrossRef] [PubMed]
6. Amgar, D.; Stern, A.; Rotem, D.; Porath, D.; Etgar, L. Tunable length and optical properties of $CsPbX_3$ (X = Cl, Br, I) nanowires with a few unit cells. *Nano Lett.* **2017**, *17*, 1007–1013. [CrossRef] [PubMed]
7. Bekenstein, Y.; Koscher, B.A.; Eaton, S.W.; Yang, P.; Alivisatos, A.P. Highly luminescent colloidal nanoplates of perovskite cesium lead halide and their oriented assemblies. *J. Am. Chem. Soc.* **2015**, *137*, 16008–16011. [CrossRef]
8. Xing, J.; Liu, X.F.; Zhang, Q.; Ha, S.T.; Yuan, Y.W.; Shen, C.; Sum, T.C.; Xiong, Q. Vapor phase synthesis of organometal halide perovskite nanowires for tunable room-temperature nanolasers. *Nano Lett.* **2015**, *15*, 4571–4577. [CrossRef]
9. Shamsi, J.; Dang, Z.; Bianchini, P.; Canale, C.; Stasio, F.D.; Brescia, R.; Prato, M.; Manna, L. Colloidal synthesis of quantum confined single crystal $CsPbBr_3$ nanosheets with lateral size control up to the micrometer range. *J. Am. Chem. Soc.* **2016**, *138*, 7240–7243. [CrossRef]
10. Li, X.; Wu, Y.; Zhang, S.; Cai, B.; Gu, Y.; Song, J.; Zeng, H. $CsPbX_3$ quantum dots for lighting and displays: Room- temperature synthesis, photoluminescence superiorities, underlying origins and white light-emitting diodes. *Adv. Funct. Mater.* **2016**, *26*, 2435–2445. [CrossRef]
11. Shamsi, J.; Rastogi, P.; Caligiuri, V.; Abdelhady, A.L.; Spirito, D.; Manna, L.; Krahne, R. Bright-emitting perovskite films by large-scale synthesis and photoinduced solid-state transformation of $CsPbBr_3$ nanoplatelets. *ACS Nano* **2017**, *11*, 10206–10213. [CrossRef]
12. Wei, S.; Yang, Y.; Kang, X.; Wang, L.; Huang, L.; Pan, D. Room-temperature and gram-scale synthesis of $CsPbX_3$ (X = Cl, Br, I) perovskite nanocrystals with 50-85% photoluminescence quantum yields. *Chem. Commun.* **2016**, *52*, 7265–7268. [CrossRef] [PubMed]
13. Wang, K.-H.; Wu, L.; Li, L.; Yao, H.-B.; Qian, H.-S.; Yu, S.-H. Large-scale synthesis of highly luminescent perovskite-related $CsPb_2Br_5$ nanoplatelets and their fast anion exchange. *Angew. Chem. Int. Ed.* **2016**, *55*, 8328–8332. [CrossRef]
14. Shi, Z.; Guo, J.; Chen, Y.; Li, Q.; Pan, Y.; Zhang, H.; Xia, Y.; Huang, W. Lead-free organic-inorganic hybrid perovskites for photovoltaic applications: Recent advances and perspectives. *Adv. Mater.* **2017**, *29*, 1605005. [CrossRef] [PubMed]
15. Zhang, Y.-W.; Wu, G.; Dang, H.; Ma, K.; Chen, S. Multicolored mixed-organic-cation perovskite quantum dots ($FA_xMA_{1-x}PbX_3$, X = Br and I) for white light-emitting diodes. *Ind. Eng. Chem. Res.* **2017**, *56*, 10053–10059. [CrossRef]
16. Lignos, I.; Morad, V.; Shynkarenko, Y.; Bernasconi, C.; Maceiczyk, R.M.; Protesescu, L.; Bertolotti, F.; Kumar, S.; Ochsenbein, S.T.; Masciocchi, N.; et al. Exploration of near-infrared-emissive colloidal multinary lead halide perovskite nanocrystals using an automated microfluidic platform. *ACS Nano* **2018**, *12*, 5504–5517. [CrossRef]
17. Yu, D.; Cao, F.; Gao, Y.; Xiong, Y.; Zeng, H. Room-temperature ion-exchange-mediated self-Assembly toward formamidinium perovskite nanoplates with finely tunable, ultrapure green emissions for achieving Rec. 2020 displays. *Adv. Funct. Mater.* **2018**, *28*, 1800248. [CrossRef]
18. Fagiolari, L.; Bella, F. Carbon-based materials for stable, cheaper and large-scale processable perovskite solar cells. *Energy Environ. Sci.* **2019**, *12*, 3437–3472. [CrossRef]
19. Shaikh, J.S.; Shaikh, N.S.; Mali, S.S.; Patil, J.V.; Beknalkar, S.A.; Patil, A.P.; Tarwal, N.L.; Kanjanaboos, P.; Hong, C.K.; Patil, P.S. Quantum dot based solar cells: Role of nanoarchitectures, perovskite quantum dots, and charge-transporting layers. *ChemSusChem* **2019**, *12*, 4724–4753. [CrossRef]
20. Wang, R.; Mujahid, M.; Duan, Y.; Wang, Z.K.; Xue, J.; Yang, Y. A review of perovskites solar cell stability. *Adv. Funct. Mater.* **2019**, *29*, 1808843. [CrossRef]
21. Quan, L.N.; Yuan, M.; Comin, R.; Voznyy, O.; Beauregard, E.M.; Hoogland, S.; Buin, A.; Kirmani, A.R.; Zhao, K.; Amassian, A.; et al. Ligand-stabilized reduced-dimensionality perovskites. *J. Am. Chem. Soc.* **2016**, *138*, 2649–2655. [CrossRef] [PubMed]
22. Philippe, B.; Jacobsson, T.J.; Correa-Baena, J.-P.; Jena, N.K.; Banerjee, A.; Chakraborty, S.; Cappel, U.B.; Ahuja, R.; Hagfeldt, A.; Odelius, M.; et al. Valence level character in a mixed perovskite material and determination of the valence band maximum from photoelectron spectroscopy: Variation with photon energy. *J. Phys. Chem. C* **2017**, *121*, 26655–26666. [CrossRef]
23. Zhang, D.; Yang, Y.; Bekenstein, Y.; Yu, Y.; Gibson, N.A.; Wong, A.B.; Eaton, S.W.; Kornienko, N.; Kong, Q.; Lai, M.; et al. Synthesis of composition tunable and highly luminescent cesium lead halide nanowires through anion-exchange reactions. *J. Am. Chem. Soc.* **2016**, *138*, 7236–7239. [CrossRef] [PubMed]
24. Nedelcu, G.; Protesescu, L.; Yakunin, S.; Bodnarchuk, M.I.; Grotevent, M.J.; Kovalenko, M.V. Fast anion-exchange in highly luminescent nanocrystals of cesium lead halide perovskites ($CsPbX_3$, X = Cl, Br, I). *Nano Lett.* **2015**, *15*, 5635–5640. [CrossRef] [PubMed]
25. Udayabhaskararao, T.; Houben, L.; Cohen, H.; Menahem, M.; Pinkas, I.; Avram, L.; Wolf, T.; Teitelboim, A.; Leskes, M.; Yaffe, O.; et al. A mechanistic study of phase transformation in perovskite nanocrystals driven by ligand passivation. *Chem. Mater.* **2018**, *30*, 84–93. [CrossRef]
26. Balakrishnan, S.K.; Kamat, P.V. Ligand assisted transformation of cubic $CsPbBr_3$ nanocrystals into two-dimensional $CsPb_2Br_5$ nanosheets. *Chem. Mater.* **2018**, *30*, 74–78. [CrossRef]
27. Imran, M.; Caligiuri, V.; Wang, M.; Goldoni, L.; Prato, M.; Krahne, R.; De Trizio, L.; Manna, L. Benzoyl halides as alternative precursors for the colloidal synthesis of lead-based halide perovskite nanocrystals. *J. Am. Chem. Soc.* **2018**, *140*, 2656–2664. [CrossRef]

28. Creutz, S.E.; Crites, E.N.; De Siena, M.C.; Gamelin, D.R. Anion exchange in cesium lead halide perovskite nanocrystals and thin films using trimethylsilyl halide reagents. *Chem. Mater.* **2018**, *30*, 4887–4891. [CrossRef]
29. Liu, H.; Liu, Z.; Xu, W.; Yang, L.; Liu, Y.; Yao, D.; Zhang, D.; Zhang, H.; Yang, B. Engineering the Photoluminescence of $CsPbX_3$ (X = Cl, Br, and I) Perovskite Nanocrystals Across the Full Visible Spectra with the Interval of 1 nm. *ACS Appl. Mater. Interfaces* **2019**, *11*, 14256–14265. [CrossRef]
30. Pan, G.; Bai, X.; Xu, W.; Chen, X.; Zhai, Y.; Zhu, J.; Shao, H.; Ding, N.; Xu, L.; Dong, B.; et al. Bright blue light emission of $Ni^{2+}$ ion-doped $CsPbCl_xBr_{3-x}$ perovskite quantum dots enabling efficient light-emitting devices. *ACS Appl. Mater. Interfaces* **2020**, *12*, 14195–14202. [CrossRef]
31. Zheng, X.; Yuan, S.; Liu, J.; Yin, J.; Yuan, F.; Shen, W.-S.; Yao, K.; Wei, M.; Zhou, C.; Song, K.; et al. Chlorine vacancy passivation in mixed halide perovskite quantum dots by organic pseudohalides enables efficient rec. 2020 Blue Light-Emitting Diodes. *ACS Energy Lett.* **2020**, *5*, 793–798. [CrossRef]
32. Chen, M.; Zou, Y.; Wu, L.; Pan, Q.; Yang, D.; Hu, H.; Tan, Y.; Zhong, Q.; Xu, Y.; Liu, H.; et al. Solvothermal synthesis of high-quality all-inorganic cesium lead halide perovskite nanocrystals: From nanocube to ultrathin nanowire. *Adv. Funct. Mater.* **2017**, *27*, 17011–17021. [CrossRef]
33. Tong, Y.; Bladt, E.; Ayguler, M.F.; Manzi, A.; Milowska, K.Z.; Hintermayr, V.A.; Docampo, P.; Bals, S.; Urban, A.S.; Polavarapu, L.; et al. Highly Luminescent Cesium Lead Halide Perovskite Nanocrystals With Tunable Composition And Thickness By Ultrasonication. *Angew. Chem. Int. Ed. Engl.* **2016**, *55*, 13887–13892. [CrossRef]
34. Pan, A.; He, B.; Fan, X.; Liu, Z.; Urban, J.J.; Alivisatos, A.P.; He, L.; Liu, Y. Insight into the ligand-mediated synthesis of colloidal CsPbBr3 perovskite nanocrystals: The role of organic acid, base, and cesium precursors. *ACS Nano* **2016**, *10*, 7943–7954. [CrossRef] [PubMed]
35. Chen, H.; Guo, A.; Gu, X.; Feng, M. Highly luminescent $CsPbX_3$ (X=Cl, Br, I) perovskite nanocrystals with tunable photoluminescence properties. *J. Alloys Compd.* **2019**, *789*, 392–399. [CrossRef]
36. Ravi, V.K.; Markad, G.B.; Nag, A. Band edge energies and excitonic transition probabilities of colloidal $CsPbX_3$ (X = Cl, Br, I) perovskite nanocrystals. *ACS Energy Lett.* **2016**, *1*, 665–671. [CrossRef]
37. Liu, H.; Wu, Z.; Gao, H.; Shao, J.; Zou, H.; Yao, D.; Liu, Y.; Zhang, H.; Yang, B. One-step preparation of cesium lead halide $CsPbX_3$ (X = Cl, Br, and I) perovskite nanocrystals by microwave irradiation. *ACS Appl. Mater. Interfaces* **2017**, *9*, 42919–42927. [CrossRef]